Biomaterials 33 (2012) 5459–5467

Contents lists available at SciVerse ScienceDirect

Biomaterials

journal homepage: www.elsevier.com/locate/biomaterials

Polyethylene glycol-based protein nanocapsules for functional delivery of a differentiation transcription factor

Anuradha Biswas [a,c], Ying Liu [d], Tianfei Liu [a], Guoping Fan [d,**], Yi Tang [a,b,c,*]

[a] Department of Chemical and Biomolecular Engineering, University of California at Los Angeles, Los Angeles, CA 90095, USA
[b] Department of Chemistry and Biochemistry, University of California at Los Angeles, Los Angeles, CA 90095, USA
[c] California NanoSystems Institute, University of California at Los Angeles, Los Angeles, CA 90095, USA
[d] Department of Human Genetics, University of California at Los Angeles, Los Angeles, CA 90095, USA

ARTICLE INFO

Article history:
Received 12 March 2012
Accepted 1 April 2012
Available online 21 April 2012

Keywords:
Transcription factor
Nanocapsule
Intracellular
Protein
Degradable
Differentiation

ABSTRACT

Transcription factors (TFs) can direct cell fate by binding to DNA and regulating gene transcription. Controlling the intracellular levels of specific TFs can therefore enable reprogramming of cellular function and differentiation. Direct delivery of recombinant TFs to target cells can thus have widespread therapeutic value, but has remained challenging due to structural fragility of TFs and inefficient membrane transduction. Here we describe the functional delivery of TFs using degradable polymeric nanocapsules to drive cellular differentiation. The nanocapsules were synthesized with poly(ethylene) glycol (PEG)-based monomers and intracellularly-degradable crosslinkers. Physical properties and release kinetics of the nanocapsules were optimized through tuning of monomer and crosslinker ratios to achieve enhanced delivery of cargo destined for the nuclei. The nanocapsules did not display cytotoxicity in primary cell lines up to concentrations of 5 μM. A recombinant myogenic transcription factor, MyoD, was delivered to the nuclei of myoblast cells using degradable nanocapsules to induce myogenic differentiation. MyoD was confirmed to be delivered to the nuclei of myoblasts using confocal microscopy and was demonstrated to be active in transcription through a luciferase-based reporter assay. More importantly, delivered MyoD was able to drive myoblast differentiation as evidenced by the hallmark elongated and multinuclear morphology of myotubes. The activation of downstream cascade was also confirmed through immunostaining of late myogenic markers myogenin and My-HC. The efficiency of differentiation achieved *via* nanocapsule delivery is significantly higher than that of native MyoD, and is comparable to that of plasmid transfection. The encapsulated MyoD can also withstand prolonged protease treatment and remain functional. The ease of preparation, biocompatibility and effective cargo delivery make the polymeric nanocapsule a useful tool to deliver a variety of recombinant TFs for therapeutic uses.

1. Introduction

Transcription factors (TFs) are modular proteins that include one or more DNA-binding domains capable of attaching to specific sequences and regulating transcription of specific genes [1,2]. As such, TFs are the primary regulatory components of cells and can determine the expression of all genes, including those imperative for cellular development and cell cycle control. The expression of specific TFs is also regulated by elaborate control mechanisms in response to different intracellular and extracellular signals [3,4]. The discovery that the diversity of different cell lineages can result from the varying combinations of TF expression has enormously impacted the field of regenerative medicine, which aims to replace diseased cells with healthy, functional cells of the same type [5,6]. For example, terminally differentiated cells have been reprogrammed into induced pluripotent stem (iPS) cells by the ectopic expression of four TFs, *Oct4, Sox2, Klf4* and *c-Myc*, which then have the capability to be differentiated into healthy functional cells of all three germ layers [7,8]. Specific TFs can also dedifferentiate cells into immature forms as evidenced by the demyelination of Schwann cells when *c-Jun* expression is increased, thereby allowing cell proliferation for replacement of damaged cells after nerve

* Corresponding author. Department of Chemical and Biomolecular Engineering, University of California, Los Angeles, CA 90095. Tel.: +1 310 825 0375; fax: +1 310 206 4107.
** Corresponding author. Tel.: +1 310 267 0438; fax: +1 310 794 5446.
E-mail addresses: gfan@mednet.ucla.edu (G. Fan), yitang@ucla.edu (Y. Tang).

0142-9612/$ – see front matter © 2012 Elsevier Ltd. All rights reserved.
doi:10.1016/j.biomaterials.2012.04.012

injuries [9,10]. Key TFs for differentiation of immature cells or transdifferentiation from different cell lineages have been identified including *CEBPα* and *CEBPβ* for macrophages [11], *Pdx1* for pancreatic β-cells [12], *Foxp3* for regulatory T cells [13] and *Ascl1, Brn2 and Myt1l* for neurons [14], etc. As a result, controlling intracellular levels of specific TFs is a powerful method to redirect cellular fate and produce healthy functioning cells of desired lineages. Developing tools to directly deliver TFs to specific cells can therefore have widespread therapeutic value in regenerative medicine.

Delivery of TFs to redirect cell fate has been explored primarily through retroviral or lentiviral methods [15–17]. These methods have raised safety concerns due to the incidence of viral integration within endogenous genomes leading to unintended gene activation [18] or transgene reactivation [19]. To address these concerns, TF delivery for generation of iPS cells has been explored using adenoviruses [20], plasmids [21,22] and transposons followed by transgene removal using Cre-mediated excision [23]. However safety issues of delivering TFs using genetic methods remain widespread due to the potential for unexpected genetic modifications by the exogenous sequences in target cells. To avoid the introduction of foreign genetic material into the cell, TFs can be introduced directly as recombinant proteins fused with protein transduction domain (PTD) tags [24,25]. However, PTD-tagged proteins suffer from inefficient escape of transduced protein from endosomes to the cytosol, degradation and inactivation of protein during the cellular uptake process [26].

To protect protein integrity and activity, and to enhance the efficiency of intracellular protein delivery, polymeric nanocarriers can be complexed to recombinant proteins using both covalent and non-covalent methods [27]. The use of polymers allows customization of the protein–polymer complexes, including tuning of overall size and surface charge, addition and presentation of responsive elements, and the installation of protective layers to preserve protein activity during cellular uptake. Nanocarrier-mediated delivery of TFs is challenging because the intricate structural features of recombinant TFs must remain intact during nanocarrier synthesis, cellular transduction and intracellular release steps [28,29]. In particular, the abundance of basic amino acid residues in the DNA-binding domains of TFs are critical for binding to the DNA-phosphate backbone, and chemical modifications to key lysines and arginines will result in loss of TF functions. Additionally, many TFs have large unstructured regions, including the DNA-binding domain, which can become structurally well-defined when interacting with specific DNA sequences or other co-activator proteins during assembly of the transcription machinery [30]. The specificity and affinity of TFs are highly reliant on preserving the native structure throughout the delivery process. Therefore for regenerative therapies, polymeric nanocarriers that can deliver recombinant TFs in native and functional form to cells are highly desired.

We have developed polymeric protein nanocapsules (NCs) to facilitate intracellular delivery of diverse proteins [31–33]. These NCs have been engineered to encapsulate proteins without covalent modification and have crosslinkers that can degrade intracellularly. To achieve intracellular release of protein, the crosslinkers are designed to be degradable only when inside the cells. We used a peptidyl crosslinker containing a highly favored substrate (RVRR) of furin, a ubiquitous endoprotease in mammalian cells [34]. Upon entry into the cell, where furin activities are abundant, the crosslinkers are proteolyzed and the polymeric matrix is degraded, leading to the release of cargo in native form. Another degradation strategy is by using a redox-responsive, disulfide-containing crosslinker *N,N'*- bis(acryloyl)cystamine [35]. The polymer shell maintains its integrity under oxidative conditions outside the cell but undergoes degradation and cargo release after entry into the more reducing cytosol. We have successfully delivered recombinant proteins to human cell lines using both furin-degradable and redox-responsive NCs. However, our approach so far is based on the less desirable polyacrylamide polymer and functional delivery of TFs has not been demonstrated to date. Here we demonstrate the synthesis, optimization and application of poly(ethylene) glycol (PEG) based protein NCs in the nuclear delivery of the TF MyoD for differentiation of myoblasts into myotubes.

2. Materials and methods

2.1. Materials

All chemicals were purchased from Sigma–Aldrich unless noted otherwise. *N*-(3-aminopropyl) methacrylamide hydrochloride was purchased from Polymer Science, Inc. CellTiter 96® AQ_{ueous} One Solution Cell Proliferation Assay (MTS) reagent was purchased from Promega Corporation. The furin-degradable peptide was synthesized as previously described [32]. Deionized water was prepared using a Millipore NanoPure purification system.

2.2. Instruments

Bradford assay absorbances were measured in a Thermo Scientific GENESYS 20 spectrometer. TEM images of nanoparticles were obtained on a Philips EM-120 TEM instrument. Zeta potential and particle size distribution were measured on the Malvern particle sizer Nano-ZS. Peptides were synthesized on a C S Bio Co. CS336X solid phase peptide synthesizer. Fluorescent images of cells were obtained with either a Zeiss Axio Observer Z1 Inverted Microscope or Leica one-photon confocal laser scanning microscope (Leica Microsystems, Heidelberg).

2.3. Protein expression and purification

NLS-eGFP was expressed and purified as previously reported [32]. For expression of MyoD, *pET-His-MyoD* (a gift from Dr. Kobatake) was transformed into BL21 cells by electroporation. Transformed cells were inoculated overnight at 37 °C with shaking in Luria–Bertani medium containing 100 μg/mL ampicillin. Overnight cultures were diluted 1:200 and grown in Fernbach flasks containing 1 L of LB medium with 100 μg/mL ampicillin at 37 °C with shaking at 270 rpm. When the cultures reached an absorbance *A*600 ~ 0.8, isopropyl β-D-thiogalactopyranoside was added to a final concentration of 1 mM to induce protein expression, and the cells were incubated for 3 h at 37 °C. The cells were harvested by centrifugation (3500 g, 4 °C, 15 min), resuspended in 30 mL Buffer A (50 mM Tris–HCl, pH 8.0, 2 mM DTT, 2 mM EDTA), and lysed by sonication. The insoluble fraction was collected by centrifugation (15,000 g, 4 °C, 30 min) and dissolved in 8 M urea overnight at 4 °C. After centrifugation at 14,000 g, 4 °C, 10 min, the solubilized fraction was filtered with a 0.45 μm filter and incubated with 3 mL of Ni-NTA resin (Qiagen) for 3 h at 4 °C. The protein was then purified using a step gradient of Buffer A with 8 M urea with increasing concentrations of imidazole (10, 20, and 250 mM). MyoD protein was eluted with 15 mL Buffer A containing 250 mM imidazole. The protein concentration was qualitatively assessed by SDS-PAGE and quantitatively determined by the Bradford protein assay. MyoD was dialyzed three times in refolding buffer (1xPBS, 1 M urea, 400 mM arginine, 40 μM glutathione (reduced), 4 μM glutathione (oxidized)) and then three times in 1xPBS. Far-UV circular dichroism (CD) spectra of MyoD protein (0.1 mg/mL in PBS) before and after refolding were obtained at 20 °C with a JASCO J-715 Circular Dichroism Spectrometer. Optical rotation was measured from 190 to 250 nm with a bandwidth of 1 nm.

2.4. Preparation of protein NCs

1 mg protein was diluted in 500 μL of 5 mM pH 9 $NaHCO_3$ buffer after which polyethylene glycol methyl ether acrylate (M_n ~ 480) was added with stirring for 10 min at 4 °C. Next, *N*-(3-aminopropyl) methacrylamide (APMAAm) was added with stirring for 5 min. Afterwards, the furin-degradable, redox-responsive (*N,N'*-Bis(acryloyl)cystamine) or non-degradable crosslinker (*N,N'*-methylene bisacrylamide) was added. The polymerization was immediately initiated by adding 3 mg of ammonium persulfate and 3 μL of *N,N,N',N'*-tetramethylethylenediamine. The polymerization was allowed to proceed for 60 min at 4 °C. Finally, buffer exchange with 100 mM HEPES, 1 mM $CaCl_2$, pH 7.5 (furin-degradable NCs) or 1xPBS (redox-responsive and non-degradable NCs) was performed to remove unreacted monomers and initiators.

2.5. Cell-free protein release assay from NCs

150 nmol of NLS-eGFP furin-degradable NC was added to 100 mM HEPES, 1 mM $CaCl_2$, pH 7.5 buffer into a total volume of 50 μL. 10 units of furin enzyme was added to the reaction mixture and incubated at 37 °C for various times. 1 unit of enzyme is

defined by Sigma as the amount of enzyme needed to release 1 pmole from flourogenic peptide Boc-RVRR-AMC in 1 min at 30 °C. 10 μg NLS-eGFP redox-responsive NC was incubated with 1 mM GSH in 200 μL PBS buffer at 37 °C for various times. Samples from specific time points were appropriately diluted for the GFP ELISA assay.

2.6. Enzyme-linked immunosorbant assay (ELISA)

To quantify native eGFP protein released, a GFP ELISA kit was obtained from Cell Biolabs, Inc., San Diego, CA. A standard curve was constructed using known eGFP amounts with the kit's standard eGFP sample and by performing the assay. Briefly, samples were centrifuged for 10 min at 7000 rpm with a 30 kDa MWCO filter to isolate native eGFP protein. Then, the samples were loaded into anti-GFP rabbit antibody coated wells and incubated at 4 °C overnight. After careful washing, a detection antibody (anti-GFP mouse antibody) was added to each well and incubated at room temperature for 2 h. Next, an anti IgG mouse-HRP conjugate antibody was added. After 1 h, TMB substrate was added and incubated for 30 min. After the addition of stop solution to each well, absorbance at 450 nm was measured.

2.7. Cell culture

HeLa and HFF (ATCC, Manassas, VA) were cultured in Dulbecco's Modified Eagle's Medium (Invitrogen) or DMEM supplemented with 10% bovine growth serum (BGS) (Hyclone, Logan, UT) or BGS, 1.5 g/L sodium bicarbonate, 100 μg/mL streptomycin and 100 U/mL penicillin. Mouse C2C12 myoblast cells (a gift from Dr. Rachelle Crosbie, UCLA) were cultured in DMEM with 20% BGS, 1.5 g/L sodium bicarbonate, 100 μg/mL streptomycin and 100 U/mL penicillin. All cells were cultured at 37 °C, in 98% humidity and 5% CO_2. Cells were regularly subcultured using 0.25% trypsin-EDTA.

2.8. Cytotoxicity study using 3-(4,5-dimethylthiazol-2-yl)-5-(3-carboxymethoxyphenyl)-2-(4-sulfophenyl)-2H-tetrazolium) (MTS) assay

Cells were seeded into 96 well plates at a density of 5000 cells per well and cultivated in 100 μL of DMEM with 10% BGS. The plates were then incubated in 5% CO_2 and at 37 °C for 12 h to reach 70–80% confluency before addition of protein/NCs. After 24 h or 48 h incubation with protein NCs, the cells were washed with PBS solution and incubated with 100 μL fresh DMEM and 20 μL MTS solution (CellTiter 96® AQueous One Solution Cell Proliferation Assay, Invitrogen). The plates were incubated for an additional 3 h. The absorbance of the plates was read at 550 nm and a reference wavelength of 690 nm using a microplate reader (PowerWave X, Bio-tek Instruments, USA).

2.9. Imaging and quantification of nuclear localization

Cells were seeded into 48 well plates at a density of 10,000 cells/well and cultured in 250 μL DMEM with 10% BGS. The plates were incubated for 12 h before being treated with 400 nM NCs. After 24 h, cells were washed 3x with PBS and fixed for 15 min with 4% paraformaldehyde. Nuclei were stained with 1 μg/mL DAPI. Cells were imaged using Z-stack imaging and Image J was used for quantification of eGFP and nuclear overlap.

2.10. Nuclear and cytoplasmic fractionation

Cells were seeded into 6-well plates at a density of 1×10^5 cells per well and cultivated in 1.5 mL of DMEM with 10% BGS. The plates were incubated for 12 h before being treated with 400 nM of appropriate NCs. Cells were collected by trypsin-EDTA and centrifugation after 24 h. A Nuclear/Cytosol Fractionation Kit (BioVision, Inc., Mountain View, CA) was used to separate cytosolic and nuclear extracts from NC-treated cells. Fractions were obtained per the manufacturer's instructions. All procedures were performed at 4 °C. Extracts were stored at −80 °C until the GFP-ELISA assay was performed (Cell Biolabs, Inc., San Diego, CA).

2.11. Protein-rhodamine conjugation

NHS-rhodamine (Thermo Scientific Pierce) was reacted with MyoD protein in a 5 molar excess in 50 mM $NaHCO_3$ buffer, pH 9 for 2 h at 4 °C. After the reaction, MyoD-rho was purified by extensive buffer exchange using PBS with 30,000 MWCO filters. MyoD-rho NCs were synthesized and cellular uptake was subsequently imaged as previously described.

2.12. MyoD luciferase reporter construct cloning

A MyoD firefly luciferase reporter plasmid was constructed using pGL3-promoter vector (Promega) as a template. Four copies of the E-box promoter sequence upstream of the firefly luciferase gene was PCR amplified using the specific primers I (5′-CTCTTACGCGTCACCTGCACCTGCACCTGCACCTGCTCGAGATCTGCGATCTGC-3′ with an underlined *Mlu*I site) and II (5′CAGTACCGGAATGCCAAGCTTTTTGCAAAAGCCTAGGCCTCC-3′ with an underlined *Hind*III site). This fragment was amplified and inserted between the *Mlu*I and *Hind*III sites of pGL3-promoter, thus resulting in *MyoD-luc*. After sequence confirmation, the plasmid was transformed into *E. coli* XL1 cells and subsequently purified by miniprep (Zymo Research).

2.13. Dual-luciferase assay

C2C12 cells were plated at a density of 10,000 cells per well in 96-well plates and incubated for 16 h. Cells were transfected with Lipofectamine per the manufacturer's instructions with 50 ng *pRL-TK* Renilla luciferase (Promega) and 0.1 μg *MyoD-luc*. For MyoD DNA transfected cells, 0.1 μg *pORFMyoD* (a gift from Dr. Derrick Rossi) was also transfected. Cells were incubated in antibiotic-free media for 4 h, after which 400 nM MyoD protein/NCs were added into fresh media with antibiotics. After 16 h, another 400 nM MyoD protein/NCs were added to cells. After a total 48 h, cells were washed three times with PBS and lysed with 80 μL Passive Lysis Buffer (Promega) for 15 min at 25 °C. Cell lysate was centrifuged at 4 °C at 3500 rpm and 10 μL was plated in a 96-well plate and luciferase activity was monitored using the Dual-Luciferase Reporter Assay system (Promega) with the GloMax Multi + Detection System.

2.14. Myoblast differentiation treatment

C2C12 cells were plated in 24 well plates (3000 cells/well) for immunostaining or 6 well plates (10,000 cells/well) for qPCR and cultured in DMEM + 20% BGS. After 24 h, cells were treated with 400 nM MyoD protein/NCs for 3 subsequent days. For MyoD transfected cells, 1 μg or 3 μg *pORFMyoD* was transfected using Lipofectamine using the manufacturer's protocol for 24 well or 6 well plates, respectively. Media was changed each day thereafter for a total of 7 days after which cells were either fixed or harvested for further experiments. For proteinase K treatment assays, 10 μg protein/NCs were treated with 50 μg/mL proteinase K in 50 mM Tris–HCl, 5 mM $CaCl_2$ pH 7.5 buffer for 1 h at 37 °C before incubation with cells.

2.15. Immunostaining

Treated C2C12 cells were washed with PBS and fixed by 4% paraformaldehyde in PBS. Immunostaining was performed with mouse anti-MyHC antibody (1:400, Millipore) and an Alexa Flour 488 conjugated secondary Ab. DAPI (0.1 mg/mL) was used for nuclear counterstaining. Positively-stained cells were counted using Image J.

2.16. Quantitative real-time PCR

Treated C2C12 cells were trypsinized, collected by centrifugation and homogenized using QIAshredder and total RNA was extracted using the RNeasy mini kit (Qiagen). RNA samples (1 μg) were treated with DNase I (Invitrogen) and reverse transcription was performed using the iScript RT kit (Bio-Rad). The SybrGreen supermix kit (Bio-Rad) was used for real-time PCR. Threshold cycle (Ct) was determined on the linear phase. Results were normalized by Ct of 18 s. Relative gene expression fold difference was calculated by $2^{-\Delta \text{normalized Ct}}$. PCR primers are listed in Table S2.

3. Results and discussion

3.1. Synthesis and optimization of PEG NCs

In order to develop an intracellular protein delivery system that is feasible for *in vivo* applications, a non-cytotoxic polymeric platform is desired. PEG is the most widely used polymer for drug delivery applications due to its biocompatibility and ability to reduce cargo aggregation and proteolysis while increasing circulation time [36]. We selected a short chain length PEG ($M_n \sim 480$) as a monomer for NC synthesis motivated by favorable properties of low molecular weight PEG including complete water solubility [37], formation of loosely packed particles [38] and easy excretion by humans [39]. A positively charged co-monomer, *N*-(3-aminopropyl) methacrylamide (M2), was also used in relatively lower quantities to provide a slight positive charge on the surface of the NC needed for cellular entry [40]. A two-step procedure is applied to fabricate the protein NCs: first, a co-monomer mixture of M2 and PEG are deposited onto the surface of target protein by adsorption; next *in situ* polymerization is initiated in an aqueous solution, containing monomers and furin or redox-responsive crosslinkers which allow intracellular degradability of NCs (Fig. 1A and B). The polymerization

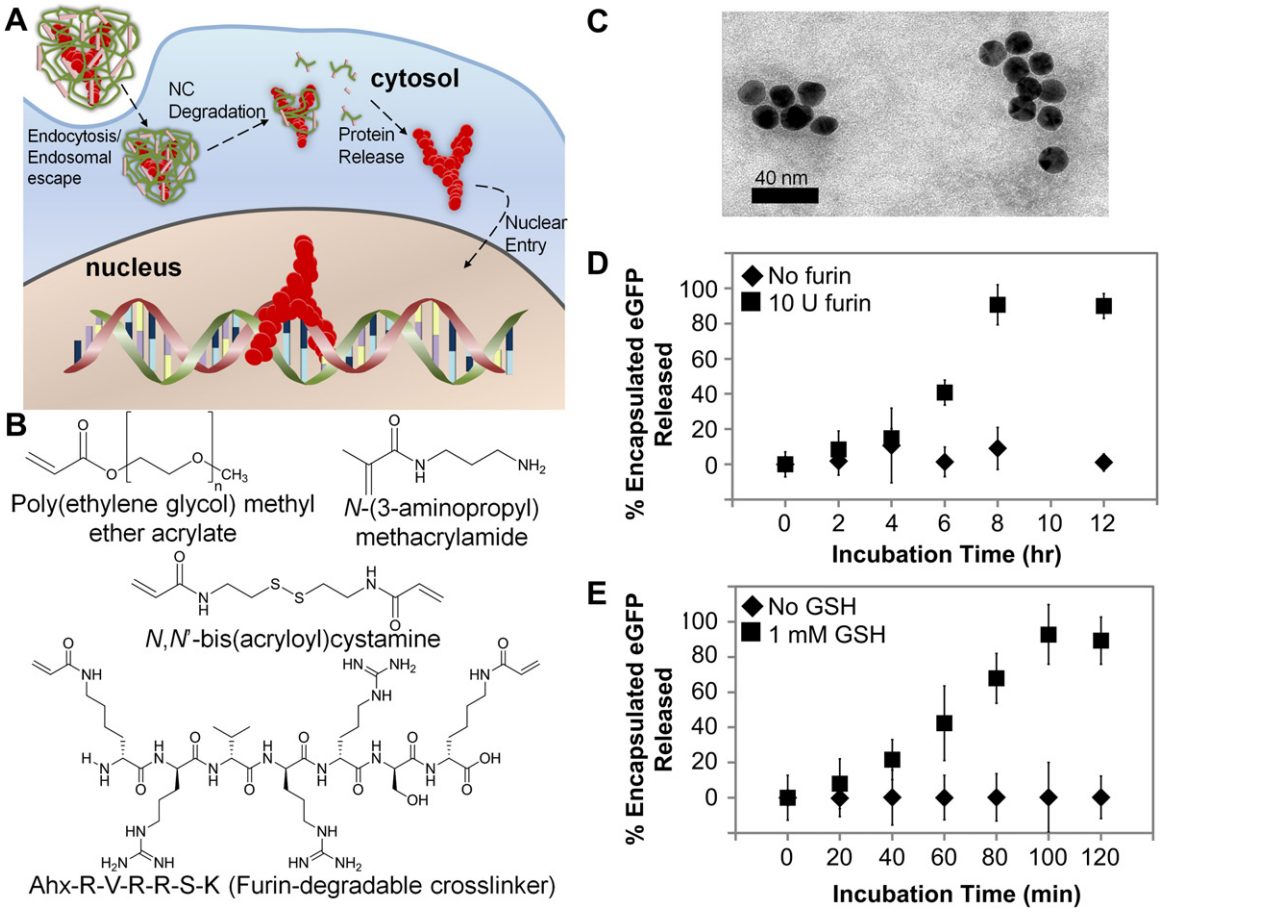

Fig. 1. Furin-degradable and redox-responsive PEG NCs can release encapsulated protein. (A) Schematic of NC-mediated TF nuclear delivery. NCs are internalized into cells, the polymeric shell degrades due to furin proteolysis or reduction in the cytosol of the crosslinker (pink), the released TF in native form localizes to the nucleus to bind DNA and initiate transcription of genes. (B) Structures of monomers and crosslinkers used for NC synthesis. (C) TEM image of redox-responsive NLS-eGFP PEG NCs. The scale bar corresponds to 40 nm. NLS-eGFP release from (D) 150 nmol furin-degradable NCs upon incubation with 10 U furin at 37 °C and (E) 10 μg NLS-eGFP redox-responsive NCs after incubation with 1 mM GSH at 37 °C at various time points quantified by ELISA. Data shown represents average values with standard deviation from three independent experiments. (For interpretation of the references to color in this figure legend, the reader is referred to the web version of this article.)

is allowed to proceed for 1 h after which unreacted small molecules are removed by ultrafiltration.

We first used nuclear localization signal-tagged enhanced green fluorescent protein (NLS-eGFP) as protein cargo to examine NC synthesis, and to establish the capability of PEG NCs to carry protein across the membrane, degrade in response to cellular cues and release protein destined for the nuclei of cells. As shown in Fig. 1C, under preparation conditions, NLS-eGFP PEG NCs are uniform and spherical in size (10–20 nm) as evidenced by transmission electron microscopy (TEM) and dynamic light scattering (DLS) (Figure S1). We further quantified the release of encapsulated protein from degradable NCs using ELISA for both furin-degradable (Fig. 1D) and redox-responsive (Fig. 1E) NCs. Upon incubation with 10 units furin or 1 mM glutathione (GSH), degradable PEG NCs released ~90% of the encapsulated NLS-eGFP protein. In contrast, NCs released <5% of NLS-eGFP without degradation stimuli indicating that the polymeric layer can maintain structural integrity when subject to incubation at 37 °C and no outward diffusion of the encapsulated cargo takes place.

We next sought to optimize the NC formulation to achieve the maximum relative content of PEG monomer while retaining cellular internalization. NLS-eGFP NCs were synthesized with varying PEG:M2 molar ratios using a non-degradable (ND) crosslinker (*N,N'*-methylene bisacrylamide). The NCs were physically characterized by DLS to determine the size and ζ–potential while uptake efficiency was measured by incubation with HeLa cells followed by visualization with fluorescent microscopy (Figures S1, S2). As shown in Figure S1, a maximum PEG:M2 molar ratio of 3.3 was determined above which the eGFP fluorescence was undetectable inside cells, presumably due to the low ζ–potential of the NCs [41]. Additionally, NC diameters and ζ–potentials were measured along with cellular uptake efficiency to establish the optimal total amount of monomers for NC formation (total moles monomers:moles protein = 21:1) (Figure S1, S2). We selected a PEG:M2 molar ratio of 2.6 which afforded NCs with the most desired properties, including an average diameter of ~10 nm, lower positive ζ–potential between 0 and 3 mV and the resulting intracellular eGFP signal as measured by fluorescent microscopy.

We next optimized the cytosolic release properties of the NCs through tuning of the crosslinking ratio (moles crosslinker: total moles monomers) (Fig. 2). The crosslinking density of NCs is a critical synthesis parameter that directly impacts intracellular degradability; a low crosslinking ratio can result in a loose polymeric matrix which "leaks" protein to the outside environment before the desired destination, whereas a high crosslinking ratio can result in a denser NC that is unable to be degraded inside the cell in a timely fashion. Using intracellular NLS-eGFP fluorescence distribution as a reporter, we can evaluate the extent of crosslinker degradation and protein release from the NCs. If the NC is unable to

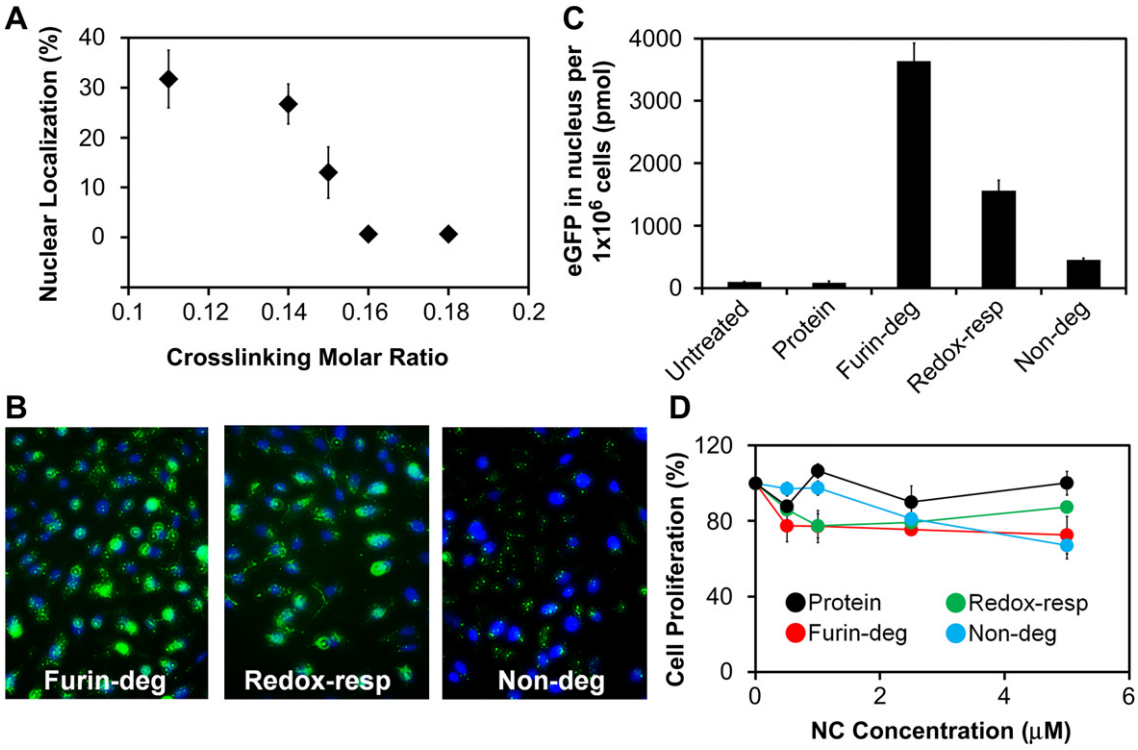

Fig. 2. Degradable PEG NCs can be engineered to deliver proteins to the nucleus. (A) Localization of eGFP with nuclei when HeLa cells were treated with 400 nM NLS-eGFP non-degradable NCs with various crosslinking ratios for 24 h before imaging. Data represents average values and standard deviation of 10 images. (B) Representative images of HeLa cells treated with NLS-eGFP NCs prepared with the same molar ratio of PEG:M2 and the same crosslinking ratio with either furin-degradable (furin-deg), redox-responsive (redox-resp) or non-degradable (non-deg) crosslinkers. Cells were treated for 24 h with 400 nM NCs before being fixed and stained. (green: eGFP; blue: DAPI-stained nuclei) (C) Quantification of eGFP in the nuclear fraction of HFF cells using ELISA. Cells were treated with 400 nM NLS-eGFP NCs prepared with various crosslinkers for 24 h before the nuclei were isolated. The data represent the average and standard deviation of three treatments. (D) Cell proliferation profiles of various concentrations of NLS-eGFP NCs delivered to HFF cells for 24 h and quantified by the MTS assay. (For interpretation of the references to colour in this figure legend, the reader is referred to the web version of this article.)

degrade intracellularly, fluorescence from NLS-eGFP will be retained in the cytosol due to inaccessibility of the NLS tag. However, upon disassembly of the NC polymeric layer and release of NLS-eGFP in the cytosol, the exposed NLS will guide the entry of the protein into the nuclei where green fluorescence can be visualized. To determine the minimal crosslinker density that can completely return protein cargo in the absence of degradation, NLS-eGFP NCs were prepared with a PEG:M2 ratio of 2.6 with varying crosslinking ratios using ND crosslinkers and delivered to HeLa cells. As shown in Fig. 2A, NLS-eGFP delivered to HeLa cells with ND NCs synthesized from a crosslinking ratio <0.16 displayed nuclear localization, likely due to the more porous polymeric matrix that enabled outward diffusion of NLS-eGFP without degradation. Near zero nuclear localization of NLS-eGFP was found when the crosslinker ratio is >0.16 when preparing ND NCs.

Using optimized PEG:M2 (2.6) and crosslinking ratio (0.16), NLS-eGFP PEG NCs synthesized with furin or redox-responsive crosslinkers were prepared. Compared to the ND NCs described above, the three different crosslinkers afforded NCs with similar physical properties (Table S1). When delivered to HeLa cells, degradable NCs afforded significant colocalization of green fluorescence in the nuclei (Fig. 2B). Optimized NLS-eGFP NCs were also delivered to human foreskin fibroblast (HFF) cells and nuclear fractions were isolated for quantification of eGFP using ELISA (Fig. 2C). Nuclear eGFP concentrations were more than 1000 fold enhanced in HFF cells treated with degradable NCs compared to cells treated with native NLS-eGFP protein which is unable to enter cells. Importantly, none of the NCs displayed significant cytotoxicity in HFF or HeLa cells up to concentrations of 5 μM, promoting the biocompatibility of optimized PEG-based NCs (Fig. 2D, S3).

3.2. NC-mediated nuclear MyoD delivery

After establishing the capability of the new PEG-based NCs as nanocarriers for nuclear protein delivery, we targeted the delivery of a recombinant TF that can drive the differentiation of specific cells. MyoD is a TF belonging to the basic helix-loop-helix (bHLH) TF family, which contains a structural motif of two α-helices connected by a loop [42]. MyoD is a master regulatory TF capable of activating muscle-specific genes and stimulating the complete myogenesis process when introduced into a large variety of cell types [43]. MyoD function is characterized to be intimately correlated with its structural integrity which has been elucidated in many previous studies; the basic DNA-binding region and α-helices must remain intact for promoter binding and dimer formation, respectively [44].

Mouse full-length MyoD protein (45 kDa) was expressed in *E.coli* BL21(DE3) cells with a polyhistidine tag, purified from inclusion bodies using affinity chromatography and refolded through extensive dialysis. Circular dichroism (CD) was performed to confirm that refolded MyoD regained the correct secondary structure content [45] (Figure S4). We subsequently synthesized MyoD NCs using the optimized PEG formulation with non-degradable and degradable crosslinkers and obtained NCs with sizes and ζ-potentials similar to each other (Fig. 3A). MyoD NCs exhibited slightly positive ζ-potentials after synthesis as desired for cellular uptake; in contrast, native MyoD displayed a negative ζ−potential before encapsulation. Interestingly, we observed decreases in sizes and size variances of MyoD NCs ($\sim$10 nm) following encapsulation when compared to native MyoD protein ($\sim$14 nm) (Figure S5). The basic region of bHLH TFs is known to be unstructured in the

A

	Mean diameter (nm)	Zeta potential (mV)
Protein	14.2 ± 6.6	-6.7 ± 1.1
Furin-deg NC	11.2 ± 3.2	2.8 ± 0.3
Redox-resp NC	11.9 ± 1.3	2.8 ± 0.4
Non-deg NC	10.2 ± 1.3	3.5 ± 0.6

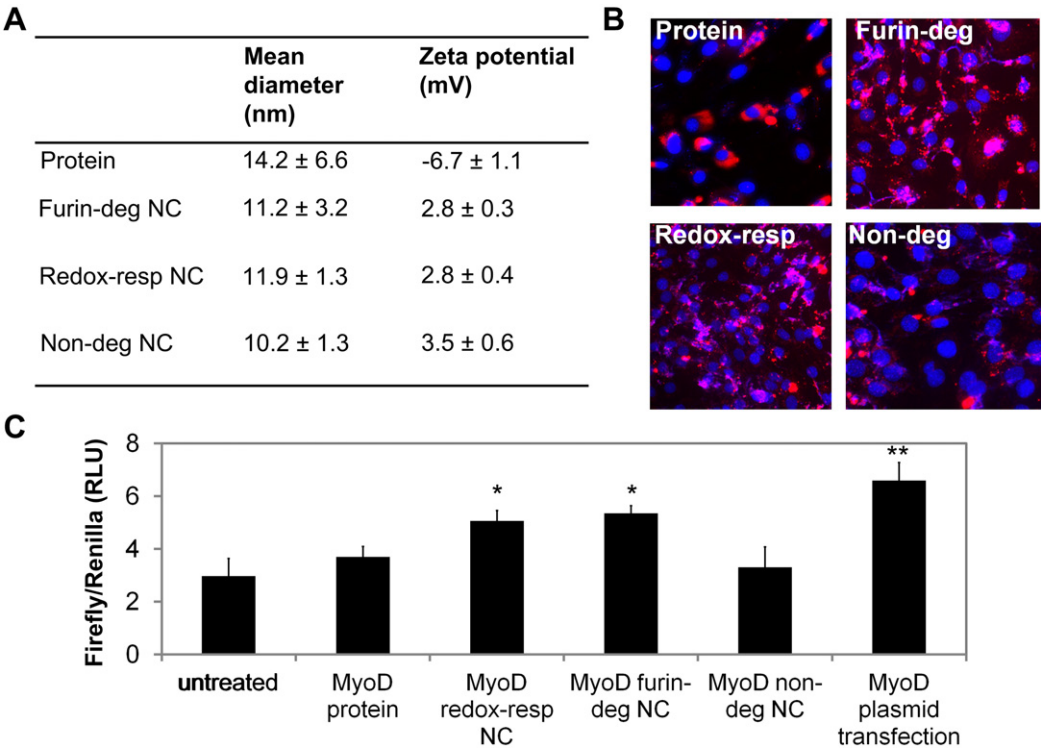

Fig. 3. MyoD protein can be encapsulated in degradable PEG NCs and delivered in active form to cells. (A) Mean hydrodynamic size and ζ−potential of MyoD protein and NCs prepared with various crosslinkers. ($n = 6$). (B) Z-stack imaging of C2C12 myoblasts which were treated with 2 doses of 400 nM rhodamine-tagged MyoD protein/NCs for 48 h before being fixed and stained. (red: rhodamine-tagged MyoD; blue: DAPI-stained nuclei; purple: nuclear colocalization) (C) Dual-luciferase assay in C2C12 cells which were transfected with a MyoD-responsive firefly luciferase construct (*MyoD-luc*) and subsequently treated with 2 doses of 400 nM MyoD protein/NCs for 48 h before cells were harvested and assayed for luciferase activity. ($n = 4$) Data is the average and standard deviation. Unpaired student *t*-test; $^{*}P < 0.05$; $^{**}P < 0.01$. (For interpretation of the references to colour in this figure legend, the reader is referred to the web version of this article.)

absence of DNA but undergoes a conformational change into α-helices when bound to cognate DNA sequences [46]. As a result, the unstructured domains of MyoD may contribute to the larger hydrodynamic radius obtained from DLS measurements. Polymerization of an encapsulating layer around MyoD may therefore serve to decrease the size of MyoD in solution by constraining motion of the unstructured regions into a more compact shape.

To examine intracellular localization of delivered MyoD in C2C12 mouse myoblast cells [47], MyoD was first conjugated to a fluorescent rhodamine dye to yield MyoD-rho prior to encapsulation. As observed by confocal microscopy (Fig. 3B), enhanced nuclear localization of MyoD-rho delivered *via* degradable NCs is observed in C2C12 cells in comparison to native MyoD-rho. As expected, MyoD-rho encapsulated in ND NCs exhibited little to no nuclear colocalization, further confirming the complete encapsulation of MyoD. These observations are consistent with previous findings indicating that native MyoD protein is able to penetrate cell membranes due to an internal PTD sequence, however nuclear localization is highly inefficient compared to those delivered by degradable NCs, likely due to protein entrapment in endosomal vesicles and degradation during cellular entry [48].

To demonstrate that MyoD delivered to nuclei by NCs was in active form, we constructed a luciferase reporter plasmid (*MyoD-luc*) containing 4 copies of the E-box sequence (CACCTG) upstream of the firefly luciferase gene. bHLH TFs are known to recognize and bind the E-box sequence to enhance transcription of downstream genes [49]. C2C12 cells were cotransfected with *MyoD-luc* and an internal control *Renilla* luciferase plasmid using Lipofectamine© and treated with 2 doses of 400 nM MyoD protein/NCs for 48 h. As shown in Fig. 3C, the levels of Firefly/Renilla luciferase expression were increased for cells treated with degradable MyoD NCs or transfected with *myoD* DNA. The lower level of increased luciferase expression may occur because the E-box sequence is not specific for MyoD and is recognized by other bHLH TFs, thereby contributing to background luciferase levels in untreated cells. Both furin-degradable and redox-responsive MyoD NC-treated cells demonstrated significant increases in firefly luciferase expression (~1.5 fold). In contrast, cells treated with native MyoD and ND MyoD NCs did not show significant increase in luciferase signals compared to untreated cells.

3.3. Differentiation of myoblast cells using degradable NCs

C2C12 myoblast cells are embryonic progenitor cells which have the potential to develop into all three muscle types: skeletal, cardiac or smooth muscle [44]. When introduced into cells from the mesoderm layer, MyoD commits cells to the skeletal lineage and further regulates the process by increasing its own expression as well as enhancing expression of other myogenic TFs and differentiated muscle proteins in a feed-forward mechanism. These cellular actions lead to myogenic differentiation and a phenotypic change from proliferating myoblasts to contractile multinucleated muscle fibers made of myotubes. Having established that degradable PEG NCs can deliver recombinant MyoD in active form to the nuclei of C2C12 cells, we devised a treatment protocol for myoblasts in which cells were treated for 3 days with 400 nM of either native MyoD protein or MyoD NCs (Fig. 4A). Subsequently, the media was changed each day until day 7 when cells were analyzed for differentiation. To test the extent of differentiation of myoblast cells into

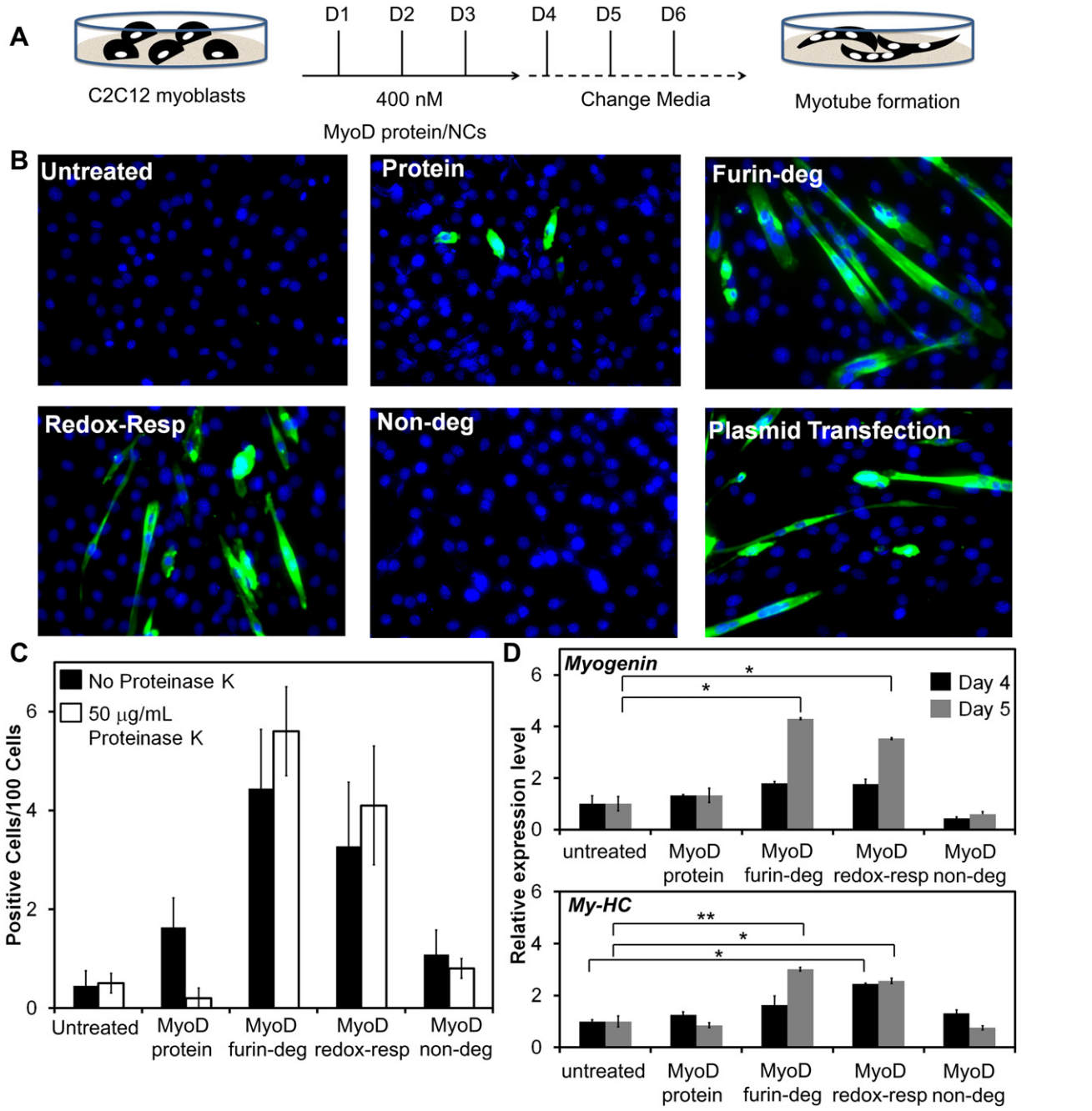

Fig. 4. C2C12 myoblasts can be differentiated into myotubes using degradable MyoD NCs. (A) Schematic of treatment of C2C12 myoblasts with MyoD protein/NCs to induce differentiation to multinucleated, elongated myotubes. (B) Fluorescent images of C2C12 cells after MyoD protein/NC treatment. Cells were immunostained with a myosin-heavy chain (My-HC) antibody conjugated with an Alexa-Fluor 488 (green). Nuclei were counterstained with DAPI (blue). (C) Quantification of positively-stained cells for each treatment group with and without 50 μg/mL proteinase K for 1 h at 37 °C. Data is the average and standard deviation of 10 images. (D) Real-time PCR analysis of the relative expression of muscle-specific genes of myogenin and My-HC in treated C2C12 cells at day 4 and day 5 of treatment. ($n = 2$). Unpaired student t-test; $^{*}P < 0.05$; $^{**}P < 0.01$. (For interpretation of the references to colour in this figure legend, the reader is referred to the web version of this article.)

mature myotubes, we performed immunostaining using a myosin-heavy chain (My-HC) antibody. My-HC is the major muscle protein of the contractile apparatus of mature muscle fibers and its increased expression is correlated with increased expression of MyoD [50,51]. As evidenced by fluorescent imaging and quantification (Fig. 4B and C), an increased number of cells exhibited My-HC expression when treated with degradable MyoD NCs as compared to cells treated with ND NCs or native MyoD protein. More excitingly, cells treated with degradable NCs also displayed elongation and multinucleation which are hallmark morphological properties of differentiated myotubes [52]. In contrast, untreated and ND MyoD NC-treated cells did not show positive staining for My-HC or morphological changes. Native MyoD protein-treated cells displayed low levels of positive staining for My-HC but did not exhibit elongated multinucleated myotubes as observed in cells treated with degradable MyoD NCs, possibly due to incomplete differentiation as a result of inefficient delivery. Notably, cells treated with degradable MyoD NCs displayed similar differentiation patterns and efficiencies to cells transfected with *myoD* plasmid using Lipofectamine©.

We further characterized the differentiation of myoblast cells by analyzing gene expression of myogenic markers My-HC and myogenin using quantitative real-time PCR at various time points during the treatment (Fig. 4D, S6, Table S2). Myogenin is an essential bHLH TF acting downstream of MyoD that coordinates skeletal muscle development into early myotubes [53]. As shown in Fig. 4D, degradable MyoD NC-treated cells showed a gradual increase in myogenin and My-HC expression and exhibited a significant increase in myogenic gene expression compared to untreated cells within 5 days after treatment. In contrast, cells treated with native MyoD and ND MyoD NCs did not exhibit significant increases in myogenin or My-HC expression within day 5. The late-stage increased expression of myogenin in MyoD protein-treated cells may be attributed to partial differentiation of myoblasts which is further supported by low expression of the later myogenic differentiation marker, My-HC observed from immunostaining and real-time PCR (Figure S6). The enhanced gene expression at earlier time points in degradable MyoD NC-treated cells may correlate to a greater quantity of functional MyoD being present in the nuclei, thereby providing the foundation to drive differentiation through cooperative association with MyoD or other related proteins to bind DNA and initiate transcription of myogenic proteins. The myogenic differentiation initiated by MyoD degradable NCs indicates that structural motifs of MyoD are preserved throughout the entire delivery and release steps. In addition to the requirement for the basic DNA-binding region of MyoD to be intact for E-box promoter binding and subsequent transcription [54–56], the α-helices of MyoD must also form homodimers or interact with the E47 co-activator to form heterodimers to activate differentiation marker expression [57–59]. Moreover, MyoD adopts different conformations in response to particular co-activators, further establishing the importance of maintaining intact MyoD structure for eventual myogenic differentiation.

3.4. Protease treatment of MyoD NCs

A desired property of nanocarriers for intracellular delivery is the ability to protect encapsulated biological components from potential degradation encountered before and during cellular entry. The unstructured regions of MyoD are targets of cellular proteases and can be inactivated upon proteolysis. To test the ability of degradable NCs to withstand external proteolysis, we incubated MyoD protein or MyoD NCs with proteinase K (PK), a broad spectrum serine protease [60]. MyoD protein or MyoD NCs were incubated with 50 μg/mL PK at 37 °C for 1 h and subsequently incubated with C2C12 cells using the differentiation treatment protocol (Fig. 4A). As shown in Fig. 4C and S7, degradable NC-treated cells persisted in forming elongated and multinucleated mature myotubes as evidenced by immunostaining and subsequent quantification. In contrast, native MyoD protein-treated cells completely lost the ability to drive the differentiation of myoblasts into myotubes, reflected in the same number of positively-stained cells as background levels (Fig. 4C). These combined results confirm the ability of polymeric NCs to shield proteins from external degradation factors such as proteolysis and retain the activity of encapsulated protein.

4. Conclusion

Intracellular delivery of recombinant TFs has extensive therapeutic impact by directing cell fate without introducing foreign genetic material into cells. The various structural components of TFs required for interacting with a plethora of macromolecular partners/targets necessitate the proteins to remain unmodified during the internalization and delivery process. In this study, we demonstrated the design, synthesis and optimization of PEG-based degradable protein NCs. Notably, PEG NCs did not display cytotoxicity in concentrations up to 5 μM, supporting the future development of degradable NCs for *in vivo* applications. We established the *in situ* polymerization strategy can package the TF MyoD into robust, spherical and sub-20 nm nanoparticles. The degradable NCs can subsequently deliver MyoD to the cytosol of myoblast cells, release functional MyoD to enter the nuclei and initiate myogenic differentiation. Importantly, PEG NCs are validated as a platform which retains encapsulated protein structure and activity as evidenced by the ability of MyoD to perform complex downstream processes and regulate myogenesis.

Acknowledgments

This work was supported by the David and Lucile Packard Foundation (Y.T.), a UCLA Broad Stem Cell Research Center Research Award (G.F.) and an NSF Graduate Research Fellowship (A.B.). We thank Dr. Rachelle Crosbie for C2C12 cells, Dr. Eiry Kobatake for *pET-His-MyoD* and Dr. Derrick Rossi for *pORFinMyoD*.

Appendix A. Supplementary material

Supplementary material associated with this article can be found, in the online version, at doi:10.1016/j.biomaterials.2012.04.012.

References

[1] Latchman DS. Transcription factors: an overview. Int J Biochem Cell Biol 1997;29:1305–12.
[2] Farnham PJ. Insights from genomic profiling of transcription factors. Nat Rev Genet 2009;10:605–16.
[3] Lobe CG. Transcription factors and mammalian development. Curr Top Dev Biol 1992;27:351–83.
[4] Vaquerizas JM, Kummerfeld SK, Teichmann SA, Luscombe NM. A census of human transcription factors: function, expression and evolution. Nat Rev Genet 2009;10:252–63.
[5] Blelloch R. Regenerative medicine - short cut to cell replacement. Nature 2008;455:604–5.
[6] Jopling C, Boue S, Belmonte JCI. Dedifferentiation, transdifferentiation and reprogramming: three routes to regeneration. Nat Rev Mol Cell Biol 2011;12:79–89.
[7] Takahashi K, Yamanaka S. Induction of pluripotent stem cells from mouse embryonic and adult fibroblast cultures by defined factors. Cell 2006;126:663–76.
[8] Wernig M, Meissner A, Foreman R, Brambrink T, Ku MC, Hochedlinger K, et al. In vitro reprogramming of fibroblasts into a pluripotent ES-cell-like state. Nature 2007;448:318–323U2.
[9] Parkinson DB, Bhaskaran A, Arthur-Farraj P, Noon LA, Woodhoo A, Lloyd AC, et al. c-Jun is a negative regulator of myelination. J Cell Biol 2008;181:625–37.
[10] Crocker SJ, Lamba WR, Smith PD, Callaghan SM, Slack RS, Anisman H, et al. c-Jun mediates axotomy-induced dopamine neuron death in vivo. Proc Natl Acad Sci U S A 2001;98:13385–90.
[11] Xie HF, Ye M, Feng R, Graf T. Stepwise reprogramming of B cells into macrophages. Cell 2004;117:663–76.
[12] Ferber S, Ber I, Shternhall K, Perl S, Ohanuna Z, Goldberg I, et al. Functional, persistent, and extended liver to pancreas transdifferentiation. J Biol Chem 2003;278:31950–7.
[13] Hori S, Nomura T, Sakaguchi S. Control of regulatory T cell development by the transcription factor Foxp3. Science 2003;299:1057–61.
[14] Vierbuchen T, Ostermeier A, Pang ZP, Kokubu Y, Sudhof TC, Wernig M. Direct conversion of fibroblasts to functional neurons by defined factors. Nature 2010;463. 1035–U50.
[15] Bian J, Popovic ZB, Benejam C, Kiedrowski M, Rodriguez LL, Penn MS. Effect of cell-based intercellular delivery of transcription factor GATA4 on ischemic cardiomyopathy. Circ Res 2007;100:1626–33.
[16] Zaret KS, Grompe M. Generation and regeneration of cells of the liver and pancreas. Science 2008;322:1490–4.
[17] Yamanaka S. A fresh look at iPS cells. Cell 2009;137:13–7.
[18] Hacein-Bey-Abina S, Von Kalle C, Schmidt M, McCcormack MP, Wulffraat N, Leboulch P, et al. LMO2-associated clonal T cell proliferation in two patients after gene therapy for SCID-X1. Science 2003;302:415–9.
[19] Okita K, Ichisaka T, Yamanaka S. Generation of germline-competent induced pluripotent stem cells. Nature 2007;448. 313–3U1.

[20] Stadtfeld M, Nagaya M, Utikal J, Weir G, Hochedlinger K. Induced pluripotent stem cells generated without viral integration. Science 2008;322:945–9.
[21] Okita K, Nakagawa M, Hong HJ, Ichisaka T, Yamanaka S. Generation of mouse induced pluripotent stem cells without viral vectors. Science 2008;322: 949–53.
[22] Kaji K, Norrby K, Paca A, Mileikovsky M, Mohseni P, Woltjen K. Virus-free induction of pluripotency and subsequent excision of reprogramming factors. Nature 2009;458. 771–U112.
[23] Woltjen K, Michael IP, Mohseni P, Desai R, Mileikovsky M, Hamalainen R, et al. piggyBac transposition reprograms fibroblasts to induced pluripotent stem cells. Nature 2009;458. 766–U106.
[24] Zhou HY, Wu SL, Joo JY, Zhu SY, Han DW, Lin TX, et al. Generation of induced pluripotent stem cells using recombinant proteins. Cell Stem Cell. 2009;4: 381–4.
[25] Kim D, Kim CH, Moon JI, Chung YG, Chang MY, Han BS, et al. Generation of human induced pluripotent stem cells by direct delivery of reprogramming proteins. Cell Stem Cell. 2009;4:472–6.
[26] Murriel C, Dowdy S. Influence of protein transduction domains on intracellular delivery of macromolecules. Expert Opin Drug Deliv 2006;3:739–46.
[27] Gu Z, Biswas A, Zhao MX, Tang Y. Tailoring nanocarriers for intracellular protein delivery. Chem Soc Rev 2011;40:3638–55.
[28] Latchman DS. Transcription-factor mutations and disease. N Engl J Med 1996; 334:28–33.
[29] Debs RJ, Freedman LP, Edmunds S, Gaensler KL, Duzgunes N, Yamamoto KR. Regulation of gene-expression in vivo by liposome-mediated delivery of a purified transcription factor. J Biol Chem 1990;265:10189–92.
[30] Dyson HJ, Wright PE. Intrinsically unstructured proteins and their functions. Nat Rev Mol Cell Biol 2005;6:197–208.
[31] Gu Z, Yan M, Hu B, Joo KI, Biswas A, Huang Y, et al. Protein nanocapsule weaved with enzymatically degradable polymeric network. Nano Lett 2009;9: 4533–8.
[32] Biswas A, Joo KI, Liu J, Zhao MX, Fan GP, Wang P, et al. Endoprotease-mediated intracellular protein delivery using nanocapsules. ACS Nano 2011;5:1385–94.
[33] Zhao MX, Biswas A, Hu BL, Joo KI, Wang P, Gu Z, et al. Redox-responsive nanocapsules for intracellular protein delivery. Biomaterials 2011;32:5223–30.
[34] Thomas G. Furin at the cutting edge: from protein traffic to embryogenesis and disease. Nat Rev Mol Cell Biol 2002;3:753–66.
[35] Meister A, Tate SS. Glutathione and related gamma-glutamyl compounds-biosynthesis and utilization. Ann Rev Biochem 1976;45:559–604.
[36] Knop K, Hoogenboom R, Fischer D, Schubert US. Poly(ethylene glycol) in drug delivery: pros and cons as well as potential alternatives. Angew Chem Int Ed Engl 2010;49:6288–308.
[37] Karakoti AS, Das S, Thevuthasan S, Seal S. PEGylated inorganic nanoparticles. Angew Chem Int Ed Engl 2011;50:1980–94.
[38] Govender T, Riley T, Ehtezazi T, Garnett MC, Stolnik S, Illum L, et al. Defining the drug incorporation properties of PLA-PEG nanoparticles. Int J Pharm 2000; 199:95–110.
[39] Webster R, Didier E, Harris P, Siegel N, Stadler J, Tilbury L, et al. PEGylated proteins: evaluation of their safety in the absence of definitive metabolism studies. Drug Metab Dispos 2007;35:9–16.
[40] Gu Z, Biswas A, Joo KI, Hu B, Wang P, Tang Y. Probing protease activity by single-fluorescent-protein nanocapsules. Chem Commun (Camb) 2010;4: 6467–9.
[41] Gratton SE, Ropp PA, Pohlhaus PD, Luft JC, Madden VJ, Napier ME, et al. The effect of particle design on cellular internalization pathways. Proc Natl Acad Sci U S A 2008;105:11613–8.
[42] Ledent V, Vervoort M. The basic helix-loop-helix protein family: comparative genomics and phylogenetic analysis. Genome Res 2001;11:754–70.
[43] Weintraub H, Davis R, Tapscott S, Thayer M, Krause M, Benezra R, et al. The myoD gene family: nodal point during specification of the muscle cell lineage. Science 1991;251:761–6.
[44] Tapscott SJ. The circuitry of a master switch: Myod and the regulation of skeletal muscle gene transcription. Development 2005;132:2685–95.
[45] Starovasnik MA, Blackwell TK, Laue TM, Weintraub H, Klevit RE. Folding topology of the disulfide-bonded dimeric DNA-binding domain of the myogenic determination factor MyoD. Biochemistry 1992;31:9891–903.
[46] Anthonycahill SJ, Benfield PA, Fairman R, Wasserman ZR, Brenner SL, Stafford WF, et al. Molecular characterization of helix-loop-helix peptides. Science 1992;255:979–83.
[47] Yaffe D, Saxel O. Serial passaging and differentiation of myogenic cells isolated from dystrophic mouse muscle. Nature 1977;270:725–7.
[48] Noda T, Fujino T, Mie M, Kobatake E. Transduction of MyoD protein into myoblasts induces myogenic differentiation without addition of protein transduction domain. Biochem Biophys Res Commun 2009;382:473–7.
[49] Lassar AB, Buskin JN, Lockshon D, Davis RL, Apone S, Hauschka SD, et al. MyoD is a sequence-specific DNA binding protein requiring a region of myc homology to bind to the muscle creatine kinase enhancer. Cell 1989;58: 823–31.
[50] Seward DJ, Haney JC, Rudnicki MA, Swoap SJ. bHLH transcription factor MyoD affects myosin heavy chain expression pattern in a muscle-specific fashion. Am J Physiol Cell Physiol 2001;280:C408–13.
[51] Muroya S, Nakajima I, Chikuni K. Related expression of MyoD and Myf5 with myosin heavy chain isoform types in bovine adult skeletal muscles. Zoolog Sci 2002;19:755–61.
[52] Charge SB, Rudnicki MA. Cellular and molecular regulation of muscle regeneration. Physiol Rev 2004;84:209–38.
[53] Armand AS, Bourajjaj M, Martinez-Martinez S, el Azzouzi H, da Costa Martins PA, Hatzis P, et al. Cooperative synergy between NFAT and MyoD regulates myogenin expression and myogenesis. J Biol Chem 2008;283: 29004–10.
[54] Hamamori Y, Wu HY, Sartorelli V, Kedes L. The basic domain of myogenic basic helix-loop-helix (bHLH) proteins is the novel target for direct inhibition by another bHLH protein. Twist Mol Cell Biol 1997;17:6563–73.
[55] Shklover J, Etzioni S, Weisman-Shomer P, Yafe A, Bengal E, Fry M. MyoD uses overlapping but distinct elements to bind E-box and tetraplex structures of regulatory sequences of muscle-specific genes. Nucleic Acids Res 2007;35: 7087–95.
[56] Bengal E, Flores O, Rangarajan PN, Chen A, Weintraub H, Verma IM. Positive control mutations in the MyoD basic region fail to show cooperative DNA binding and transcriptional activation in vitro. Proc Natl Acad Sci U S A 1994; 91:6221–5.
[57] Ishibashi J, Perry RL, Asakura A, Rudnicki MA. MyoD induces myogenic differentiation through cooperation of its NH2- and COOH-terminal regions. J Cell Biol 2005;171:471–82.
[58] Etzioni S, Yafe A, Khateb S, Weisman-Shomer P, Bengal E, Fry M. Homodimeric MyoD preferentially binds tetraplex structures of regulatory sequences of muscle-specific genes. J Biol Chem 2005;280:26805–12.
[59] Lluis F, Ballestar E, Suelves M, Esteller M, Munoz-Canoves P. E47 phosphorylation by p38 MAPK promotes MyoD/E47 association and muscle-specific gene transcription. EMBO J 2005;24:974–84.
[60] Ebeling W, Hennrich N, Klockow M, Metz H, Orth HD, Lang H. Proteinase K from Tritirachium album limber. Eur J Biochem 1974;47:91–7.